Absence of mechanical loading in utero influences bone mass and architecture but not innervation in Myod-Myf5-deficient mice.

Cédric Gomez, Valentin David, Nicola M Peet, Laurence Vico, Chantal Chenu, Luc Malaval, Timothy M Skerry

Absence of mechanical loading in utero influences bone mass and architecture but not innervation in Myod-Myf5 deficient mice.

Cédric Gomez[1,2], Valentin David[1], Nicola M. Peet[2], Laurence Vico[1], Chantal Chenu[2], Luc Malaval[1], Timothy M. Skerry[2,3]

1: INSERM, E0366, Saint-Etienne, France; IFR62, Lyon, France ; Université Jean Monnet, Faculté de Médecine, Saint-Etienne, France

2: Department of Veterinary Basic Sciences, Royal Veterinary College, London, United Kingdom

3: Present address : Academic Unit of Bone Biology, Division of Clinical Sciences, School of Medicine & Biomedical Sciences, Sheffield, United Kingdom

Abbreviations:

dd/ff: MyoD$^{-/-}$/Myf5$^{-/-}$ mice, NP-1: Neuropilin-1, PGP 9.5: Protein Gene Product 9.5, Plx: Plexin, ROI: Region of interest, Sema-3A: Semaphorin-3A, TRACP: Tartrate Resistant ACid Phosphatase; VIP: Vasoactive Intestinal Peptide, WT: Wild Type mice.

Abstract

While responses of bone to increased loading or exercise are well studied, understanding of the effects of decreased usage of the skeleton has been limited by the scarcity of suitable models. Such models should ideally not affect bone innervation, which appears to be a mediator of physiological responses of bone to unloading. MyoD-/- / Myf5-/- (dd/ff) mice lack skeletal muscle, so the fetuses develop without any active movement in utero and die soon after birth. We used micro-CT and histology to analyse their bone development and structure during endochondral ossification in parallel with the establishment of bone innervation. Long bones from mutant mice were profoundly different from controls, with shorter mineralised zones and less mineralisation. They lacked many characteristics of adult bones – curvatures, changes in shaft diameter, and traction epiphyses where muscles originate or insert, that were evident in the controls. Histologically, dd/ff mice showed the same degree of endochondral development as wild type, but presented many more osteoclasts in the newly layed bone. Innervation and the expression pattern of semaphorin-3A signaling molecules were not disturbed in the mutants. Overall, we have found no evidence for a major defect of development in dd/ff mice, and specifically no alteration nor delay in endochondral ossification and bone innervation. The altered morphological features of dd/ff mice and the increased bone resorption show the role of muscle activity in bone shaping and the consequences of bone unloading.

Introduction

Bone is a dynamic tissue that can adapt its mass and architecture to external mechanical loads. While responses of bone to increased loading or exercise are well studied (if still incompletely understood), understanding of the effects of decreased usage of the skeleton has been limited by the scarcity of suitable models. Experiments using limb casting (Uhthoff & Jaworski, 1978), showed the principle of bone's atrophy in response to disuse, that were confirmed in humans very effectively by studies of bed rest and astronauts in free fall (Whedon, 1984; Vico et al., 2000). However, the most widely used animal model for disuse has been surgical section of the sciatic nerve in rodents, which has the added complication of alterations to autonomic supply to the limb (Weinreb et al., 1989). In the light of the recent discoveries of the role of the nervous system in regulation of bone mass/architecture (Chenu, 2004; Elefteriou & Karsenty, 2004), it was necessary to devise a model in which the innervation remained intact. In addition, the rationale for studying interactions between the skeleton and the nervous system is strong. The existence of a functional innervation of the bone tissue is well known (Gronblad et al., 1984; Hohmann et al., 1986; Bjurholm et al., 1988; Serre et al., 1999) and neural influences on bone growth, remodelling and repair are also clear (Edoff et al., 1997; Sandhu et al., 1987; Cherruau et al., 1999). Furthermore, the mechanisms behind leptin-dependant regulation of bone mass have been determined to be via a hypothalamic relay to the autonomic nervous supply to the skeleton (Ducy et al., 2000; Takeda & Karsenty, 2001). Recent studies show that mechanical loading locally increases bone innervation (Wada et al., 2001), and the adrenergic part of the sympathetic nervous system appears as a mediator of the physiological response of bone to unloading (Levasseur et al., 2003; Kondo et al., 2005). The mechanisms involved in the regulation of formation of the innervation of bone have not been determined. In the central nervous system, many studies have described families of proteins

involved in nerve guidance, among which are the Semaphorins, a large family of cell surface and secreted proteins. Since there is now a substantial literature on the expression and function in bone of molecules traditionally considered to be involved in central neurotransmission (Spencer et al., 2004; Bliziotes et al., 2002; Sisask et al., 1996; Sisask et al., 1995), this may be less of an iconoclastic finding than it first appears.

The current experiments were initiated by the need to understand better the role of disuse in bone development. For this reason, we chose to determine the effect of the absence of active movement of fetuses in utero on skeletal development. Previous human infant studies suggest that this would be a possible model for disuse, since it has been shown that children born with muscular dystrophies which affect fetal movement (fetal akinaesias), have bones that exhibit signs of disuse – thin cortices, and low mineralisation of the bone tissue (Rodriguez et al., 1988; Chen et al., 1995). Rudnicki et al. developed mice lacking the genes for the transcription factors Myo-D and Myf-5, which when interbred, produced offspring that were incapable of forming functional striated muscle (Rudnicki et al., 1993). Development of the muscles of these animals had been studied, but little skeletal analysis had been performed. Here we have analysed the skeletal phenotype of the double knockout mice more fully and established them as a good model for disuse in bone development. Specifically, we have used the mice to determine whether the lack of embryonic movement exerts an influence on the development of bone innervation which could impact on skeletal development. We show that despite profound effects of developmental disuse on bone mass and architecture, and the major influence of the nervous system on the skeleton postnatally, the development of the innervation of bone is not different in the skeletons of mice that are incapable of movement.

Material and Methods

Animals

The Myo-D and Myf-5 mouse strains were provided by Dr Michael Rudnicki of McMaster University, Hamilton, Ontario, Canada. Both were on a C57B6 background. Myo-D null mice are phenotypically silent and can be bred as homozygotes successfully for many generations. The mice used in these studies have been bred for over 10 generations, so can be considered to be congenic. Homozygous Myf-5 null mice are not viable at birth, because of truncations of the ribs and muscle abnormalities. For this reason, the transgenic strain is maintained in heterozygotes, so each generation is genotyped to determine parents for the next offspring. For reasons that are not known, the vigour and viability of these mice diminishes with successive generations, and in order to perform these studies, a new C57B6 male was bred into the strain approximately every 15 generations. The mice were then bred for 3-4 generations before crossing with Myo-D null mice to generate double heterozygotes.

Pregnant females were killed by vertebral extension, in accordance with the local Ethical Committee recommendations and E14 and E18 fetuses were collected immediately post mortem. Tail samples were collected and processed for genotyping. Whole embryos or excised limbs were fixed in 4% formaldehyde in 0.1M phosphate buffer, pH 7.3 at 4°C for 24h (McKee et al., 1991).

Genotyping

DNA was extracted from tail samples with a DNAesy kit (Qiagen). Polymerase chain reaction was performed in order to detect the PGK-NEO cassette inserted in exon I of *Myf5* (Forward primer: CCAAGGTGGAGATCCTCAGG; Reverse primer: TCATAAAGTGGCAAGACAGT) and to attest the absence of *MyoD* (Forward primer:

CTTCTATGATGATCCGTGTTTCAGC; Reverse primer: CTGGACACCTTCGATGTAGCG). The number of the different genotypes represented in generations of Myf-5 +/- intercrosses, Myo-D -/- Myf-5 +/- crosses and the final double heterozygote crosses was recorded and compared with the expected Mendelian ratios.

Whole mount preparation

The pups were skinned and eviscerated, fixed in 90% ethanol for seven days, and then stained in 0.1M Alcian Blue solution in ethanol containing 20% glacial acetic acid for 3 days at room temperature. After rehydration in graded ethanol, the pups were stained in alizarin red solution (0.025M) for 3 days, and then cleared in 1% KOH until the skeletons were visible.

Skeletal morphometry

The size of two traction epiphyses were measured. The deltoid tuberosity is the skeletal site of origin of the brachialis muscle, which is responsible for flexion of the elbow joint. The olecranon is the proximal end of the ulna where the triceps muscle inserts to extend the elbow, a function vital for weight support in quadrupeds. The deltoid tuberosity size was measured by taking measurements of the humeral diameter immediately above and below the tuberosity and of the distance from the most prominent extent of the tuberosity to the opposite side of the humerus. The mean humeral diameter was subtracted from the measurement of the tuberosity plus the humerus. The protrusion of the olecranon was assessed by holding the elbow joint so that the humerus and ulna were at 90^{o} to each other, and capturing a lateral image of the limb. Using image analysis, the distance from a line drawn on the caudal aspect of the humerus to the proximal extent of the olecranon was measured. Bone lengths and diameters measures were made of the left forelimb bones using a precision engineering micrometer (Mitutoyo, Japan). Diameters were measured in the antero-posterior plane.

High resolution µCT

Fixed and ethanol-dehydrated whole embryos and hind limbs were scanned with a high resolution µCT (Viva CT40, Scanco Medical, Bassersdorf, Switzerland). Data were acquired at 45 KeV with a 10µm cubic resolution. Three-dimensional reconstructions of femurs were generated using the following parameters: Sigma: 1.2, Support: 2, Threshold: 150. After reorientation, virtual transverse and longitudinal sections were performed on femur 3D reconstructions. Femoral width at mid-diaphysis was measured on medial longitudinal sections. Cortical thickness was calculated by integration of the value on each transverse section. Linear attenuation coefficient was averaged on the whole femur reconstruction and on an area restricted to the bone collar, as subtracted by an iterative ROI-generation procedure.

Tissue processing

For histology, undecalcified embryos were embedded in methylmethacrylate and longitudinal coronal slices of the limbs were cut with a Jung model K microtome (Carl Zeiss, Heidelberg, Germany). Eight µm thick sections were used for modified Goldner staining, Von Kossa staining of mineral, with neutral red counter staning (O'Shea et al., 2003) and TRACP enzymatic staining of osteoclasts, not counter-stained (Janckila et al., 1978). For immunnocytochemistry, excised limbs were decalcified in di-sodium ethylenediamine-tetra-acetic acid (EDTA) for 2 (E14) to 6 (E18) weeks before dehydratation through a graded ethanol series, soaking in methylcyclohexan, and then paraffin embedding.

Osteoclast quantification

TRACP-labelled osteoclasts were counted under a Leica DMRB microscope (Leica, Paris, France) on approximately longitudinal and non successive sections of individual tibia and

fibula, and the number normalized on the total area of the bone section measured with the Biocom image analysis software (Explora Nova, La Rochelle, France). The data from 4 to 8 sections were averaged for each bone sample.

Immunocytochemistry

Sections of paraffin blocks were on a Leica RM2145 microtome (Leica instruments, heidleberg, Germany) and laid on silanized slides to dry overnight at 37°C. After two baths of methylcyclohexan and rehydratation, sections were treated for 15min with 100mM glycine and 50mM ammonium chloride in 50mM tris buffer, pH 7.6, in order to saturate free aldehydic groups. Endogenous peroxydase activity was inhibited by 15min incubation with 1% sodium azide and 1.5% H2O2 in 50% methanol. Sections were incubated overnight with primary antibody diluted in Tris Buffer Saline (TBS: Tris-HCl 50mM, pH: 7.6, 0.9% NaCl, 0.01% BSA) Goat polyclonal antibodies were purchased from Santa-Cruz (Santa-Cruz, CA, USA) and used at final dilutions of 1/25 (anti human Plx-A2 sc-10144), 1/50 (anti rat Sema-3A sc1148, anti human NP-1 sc-7240, anti human Plx-A3 sc-10134), 1/100 (anti human Plx-A1 sc-10139) or 1/500 (anti mouse VIP sc-7841). A rabbit anti human PGP9.5 polyclonal antibody-(AB5925) was purchased from Chemicon (Temecula, CA, USA) and used at 1/4000. Controls were incubated with non-immune goat or rabbit serum. Labelling with goat primary antibodies was followed by a 30min incubation with a rabbit anti-goat IgG (Dako, Copenhagen, Denmark). Antibody/antigen complexes were then detected with a rabbit Dako EnVision+ K4002 kit (Dako, Copenhagen, Denmark). Labeling was revealed with 3-3' diaminobenzidine tetrahydrochloride (DAB) vectastain SK4100 (Vector Laboratories, Burlingame, CA, USA). All washing were done with TBS containing 0.04% Tween 20. Sections were dehydrated, mounted in XAM, and then observed on a Leica DMRB microscope (Leica).

Statistical analysis

Morphometry and μCT data were analysed using the Mann-Whitney U test. Osteoclast densities were assessed with 2 way (genotype and bone type) ANOVA with Bonferroni post-test. All results are given as Mean±SEM of data from 3 to 6 fetuses.

Results

Incidence of dd/ff offsprings

The comparison of numbers of predicted and actual genotypes of Myf-5+/- offspring was not easy. If the dams were disturbed soon after parturition, they were inclined to eat their offspring, both the dead homozygous null mice and the other viable ones. However, it appeared that Mendelian ratios were preserved, with 1 +/+:2+/-:1-/- in the litters. Similar problems were experienced in the Myf-5 +/- Myo-D -/- crosses but again there was not large deviation from expected equal numbers of double heterozygotes and Myf-5+/+ Myo-D+/- offspring. As the final double heterozygote crosses were not allowed to proceed to term, we obtained good data on the exact numbers of the different genotypes of offspring. Instead of the expected 1:16 ratio, we obtained only 6 dd/ff offspring out of a total of 298 pups, a ratio of 1:50. After these early parts of the work, it became apparent that normal rib development could be used as a marker to exclude most of the unwanted genotypes, so we only genotyped animals with abnormal ribs. Additional data were not collected on numbers subsequently, but the incidence of dd/ff pups was not noticeably different.

Skeletal morphometry

There were no significant differences in the length of the humerus and radius of the wild-type (WT) and dd/ff mice (Table 1). The ulnae of the dd/ff mice were significantly shorter by approximately 10% (Table 1) but this difference was due entirely to reduction in the length of the olecranon, and not the shaft of the bone between elbow and carpal joints. The diameters of the ulnae and radii were not significantly different between the WT and dd/ff mice although the bones of the dd/ff mice appeared to be smoother and had fewer surface features. We could not find a way to assess this objectively. The humeral diameters of the two groups were different though. The humeri of the WT mice had the characteristic sigmoid shape when

viewed laterally, with flared proximal and distal metaphyses to provide wide joint surfaces and a relatively narrow midshaft diameter. In contrast, the dd/ff mice had humeri that did not vary significantly between the proximal middle and distal regions of the bone and lacked the curvatures of the WT bones.

µCT analysis

Images of whole mount preparations of pups as well as 3D µCT reconstructions of the whole skeleton of E18 mice clearly show that dd/ff mutants are smaller in size and shorter limbed than WT mice and lack almost completely the ribs (figure 1). Skull bones also appear to be less mineralized or less developed in mutants. Images of longitudinal and transverse section of femurs were generated by spatial reorientation of the original 3D reconstructions. As shown on Figure 2A, the images show the smaller size of mineralized femoral shaft. The cortical area of E18 femurs encompasses an outer, porous area and an inner, denser layer which can be identified as the original bone collar (Figure 2A, arrows). Maximal width at midshaft was measured on longitudinal sections while cortical thickness was assessed on thresholded 3D reconstructions of long bones. As shown on Figure 2B, both parameters were significantly higher in mutants than in wild-type mice, findings consistent with the analysis of forelimb morphology. The linear attenuation coefficient of scanned structures is an index of their degree of mineralization. We measured those parameters in the whole reconstructed femur and in a volume restricted to the bone collar. In both genotypes, the degree of mineralization was higher in the bone collar; whole femur and bone collar mineralization were significantly lower in dd/ff mice (table 2).

Bone tissue development and activity

Histology did not show any structural difference or developmental delay in bone formation at E14, when only cartilage condensations were present in limbs (data not shown). Similarly, at E18, chondrocyte hypertrophy in the phalanx was as developed in dd/ff than in WT mice (figure 3A, B). Goldner-stained leg sections confirmed that muscles are effectively absent in dd/ff compared to WT mice (figure 3D). However, ossification was equally developed and structured in the long bones of either genotype. Enzymatic staining for TRACP, a specific marker of osteoclasts, and counting of positive cells revealed that, on average, mutant mice have 2 to 4 time more osteoclasts in limb bones than WT mice (figure 3E, F and D).

Bone innervation

At E14, both dd/ff and WT mice showed the same pattern for nerve marker labeling in terms of either extent of positive labeled areas or details of cell specific expression. Labeling for PGP 9.5, a general neuronal marker, revealed nerves fibers in the periosteum facing the hypertrophic chondrocytes (figure 4A, doted line circles). Nerves fibers were also present in association with blood vessels (arrows) and intimately with osteoblasts (arrowheads). Vasoactive intestinal peptide (VIP) expression was also used to identify nerves. VIP is often conveyed by sympathetic nerve fibres. VIP immunoreactive nerve fibers were clearly present in the periosteum, in association with blood vessels (figure 4B, arrows). Similarly to E14, we could not detect any major difference in innervation at E18 between WT and dd/ff mice. In the metaphysis and the diaphysis (figure 4C and D respectively), PGP 9.5 was expressed in blood vessels (arrows). In both areas nerves fibers were densely present around bone cells lining bone trabeculae under the growth plate and in the endosteum. In the metaphysis, PGP 9.5 was also strongly expressed in contact with periosteal osteoblasts and in the periosteum (figure 4C), while VIP was detected in blood vessels (Figure 4F, arrows) and labeled strongly

nerves fibers surrounding bone cells under the growth plate. In the diaphysis, VIP was strongly expressed on and around bone cell lining bone trabeculae (Figure 4G).

All Sema-3A-signaling molecules were found to be expressed with the same pattern in WT and dd/ff mice. At E14 Sema-3A (figure 5A) and its receptor NP-1 (not shown) were expressed in hypertrophic chondrocytes as well as in resting chondrocytes in the forelimb. Co-receptors Plx-A1 and A2 were not detected at this stage. Plx-A3 was detected in blood vessels (data not shown). At E18, in the metaphysis, Sema-3A was still expressed by hypertrophic chondrocytes (not shown), by most cells under the growth plate, and in the periosteum (figure 5B). In the diaphysis Sema-3A was found in blood vessels (figure 5C, arrows), osteoblasts (short arrows) and nerves (arrowheads). In the metaphysis, most cells under the growth plate were stained for NP-1 (figure 5D). In the diaphysis NP-1 was present in some osteoblasts (figure 5E, short arrows) and in blood vessels (encart). Plx-A1 was present in most bone cells and osteocytes; it was also expressed in the periosteum (figure 5F) and in blood vessels (figure 5G, arrows). Plx-A2 was found in blood vessels (figure 5H and I, arrows) and in some osteoblasts in the diaphysis (short arrows) and metaphysis, it was also found to be expressed by nerve fibers (arrowheads). Plx-A3 was expressed in blood vessels (figure 5J and K, arrows) and the staining formed a network around bone cells as do typically nerve markers. In summary, expression of markers of innervation and Sema3A signaling was identical in terms of pattern and intensity in both genotypes.

Discussion

While this paper was being prepared, Rot-Nikcevic and coworkers (Rot-Nikcevic et al., 2006) published a detailed anatomical description of the skeleton of dd/ff mice. In addition to the same changes in long bone shape, morphometry and features described here, their work documents and discusses extensively the effects of the mutations on cranial and ribcage morphology. The study highlights the fusion of several cervical vertebrae, smaller and cleft sternum and heteromorphic clavicles in the dd/ff mutants. Interestingly, these authors observed little change of the neurocranium, while the viscerocranium (face) of the mutants is much affected. They describe a retrognatia with shorter zygomatic arches and mandible, as well as unfused and cleft palate which can be directly attributed to the lack of striated muscles (in the latter case, in the tongue). Our own study focused on the appendicular skeleton of dd/ff mice, and is the first work scrutinizing endochondral development as well as mineralization, cellular dynamics and innervation of long bones in the absence of striated muscles.

The large difference between predicted and actual numbers of offspring of the double heterozygote matings suggests that dd/ff pups are not able to develop normally to term. Because even the predicted ratio of 1:16 means that it is unlikely that any single mating will result in more than one affected pup, a full study of this phenomenon will require a substantial breeding programme to acquire uteri at various stages of pregnancy if the cause of this is to be known. We can only speculate that some process after fertilisation requires the function of both Myo-D and Myf-5. The relatively normal ratios of other matings suggest that either gene can substitute for this function, whatever it may be.

The effect of the dd/ff genotype was profound. In pups taken from uteri post mortem, movement was seen in most pups before they were euthanased. However those that later were shown to have abnormal ribs and the dd/ff genotype did not move, and had a wasted

appearance due to the lack of any bulk of muscle tissue under the skin. Because movement, wasted appearance and rib abnormalities were such good predictors of genotype, in later studies only a subset of the pups were retained and genotyped to save time and costs.

In the initial papers describing the phenotypes of the Myo-D and Myf-5 homozygous deletion mice, there was significant note taken of the lack of development of the distal parts of the ribs in Myf-5 -/- mice. When the first dd/ff mice were generated in the muscle studies by the originators of the strains, it was assumed that the dd/ff were not viable because their Myf-5 genotype was causing the same abnormal rib development as in mice with at least one Myo-D allele. Here we suggest that the rib phenotype is much more severe in dd/ff than in Myf-5 -/- mice as there is almost complete absence of the ribs in dd/ff. This aberrant rib development was initially thought to reflect a role for the myotome in skeletal patterning. It has been shown since that mice with knock-in or CRE-driven inactivations of the *myf5* gene have apparently normal ribs -pending a thorough analysis of their skeletal phenotype (Kaul et al., 2000). This is in contrast with the homozygous deletion used in the present study, in which lack of ribs may reflect a distal effect of this specific mutation on one or several unknown genes (Kaul et al., 2000).

The absence of functional skeletal muscle in the dd/ff mice is clear and unequivocal. The effect this has on the skeleton is equally profound, as demonstrated by the different analyses we have made. Although mutant mice are smaller in size; the individual bony elements of the entire skeleton and well defined joints are recognizable and identifiable because of their anatomic form. However this form is not normal. Skull bones appear to be less mineralized and less developed in mutants; long bones have a shorter mineralized shaft and are much less curved than in WT mice, suggesting that function in utero is responsible for many anatomical features evident at birth. Perhaps unsurprisingly, the deltoid tuberosity, which is a significant feature of the humerus, is hard to detect in the dd/ff, and its reduction in size is highly

significant. The olecranon is less profoundly affected, but clearly the lack of movement during development is associated with significant reduction in growth of the proximal ulna. This reduction in these traction epiphyses is particularly strong evidence for the bone phenotype of dd/ff mice being an effect of altered mechanical loading rather than any other indirect effect of the deletion. It has been accepted for decades or even centuries that traction epiphyses develop in response to pull from the muscles during development (Wolff, 1892), but our own work is the first direct evidence for this. While we measured only the deltoid tuberosity and olecranon, there were similar effects on traction epiphyses in the hind limb. That the long bones were straighter is another phenomenon known to be an effect of disuse (Lanyon, 1980; Biewener & Bertram, 1994). Because this effect was different in the different long bones we could not devise an objective measure of straightness, but the images of the humeri provide clear illustration of this difference.

In contrast to morphological effects, the pace of long bone development, as assessed by histological observations, was not altered on dd/ff fetuses. However, a strong increase in numbers of TRACP positive cells was observed in dd/ff mice. Stimulation of bone resorption is largely documented for limb unloading in the literature (Grano et al., 2002), although to our knowledge we are the first to describe it in developing fetal bone. Structural and quantitative study of dd/ff femur 3D reconstructions surprisingly revealed an increase in total width and cortical thickness, which are generally decreased in bone unloading models (Wronski & Morey, 1982; Basso et al., 2005; Yonezu et al., 2004), as well as a decrease in matrix mineralization. Few studies have been devoted so far to the effects of hypogravity (Kawashima et al., 1995) or hypokinesis (Hosseini & Hogg, 1991) on fetal bone development. Curarized rat fetuses, a model of Fetal Akinesia Deformation Sequence (FADS), are subjected to loss of mobility and partial loss of muscle strain. Fetuses treated from E17 and analysed at E21 have a decrease in body weight and size, as well as reduced femoral cross section,

femoral cortical area, and diaphyseal perimeter (Palacios et al., 1992). The latter contrasts with our data, but it is not possible to exclude in these experiments a direct effect of D-tubocurarine on bone cell activity (Walker et al., 2001). Amniotic liquid puncture, another model of FADS, did not induce any bone alteration (Palacios et al., 1992), suggesting that muscular strain more than kinesis is the main mechanical factor regulating fetal bone modelling. In dd/ff mice, the increased cortical width suggests an acceleration of osteoblastic bone formation which may lead to the deposition of an altered, hypomineralized matrix as described for instance in Paget's disease of bone (Schneider et al., 2002). This may be a real reflection of the adaptive response in the skeleton. The idea that loading induces bone formation and disuse resorption is very simplistic because adaptations to loads involve more complex effects. For example, in response to applied loading, the naturally curved rodent ulna first becomes straighter, as a result of cessation of modeling drifts (Mosley et al., 1997). In many parts of the bone this is seen as a reduction in width and thickness which would intuitively seem to be an inappropriate response. However the effect is either to increase the bone's resistance to the specific loading being applied or improve the predictability of failure (Bertram & Biewener, 1988). So the apparently greater cortical thickness and width in the KO mice may be the "genetic baseline" mass and architecture that is modified in the wild type mice by the effects of activity. Admittedly other specific consequences of the mutation may also play a part here. While the absence of muscle tissue is unlikely to affect bone shortening or increased resorption, which are documented in other immobilisation models where the muscle mass is maintained (Pitsillides, 2006; Thompson & Rodan, 1988), a specific trophic effect on cortical bone growth, although very unlikely, cannot be ruled out. Also, a cis effect of the myf5 mutation on one or several unknown genes as described by Kaul et al (Kaul et al., 2000) may have affected bone formation. In this respect, an analysis of the skeletal phenotype of other myf5-invalidating mutations would be interesting.

We have previously demonstrated the expression of the Sema-3A signaling molecules by rat bone cells and shown that their signaling precedes or coincides at the temporal but also spatial level with endochondral ossification and bone innervation in rats, suggesting a role for Sema-3A in these processes (Gomez et al., 2005). In long bone, rat nerve fibers appear in the periochondrium of the diaphysis as early as E15 (approximately E13.5 for mice) and become functional at E18-19 (approximately E16-17.5 in mice) (Sisask et al., 1995; Sisask et al., 1996). Immunocytochemical study revealed that Sema-3A and NP-1 are expressed in the same fashion in dd/ff and WT mice from E14 in the cartilage anlage to E18 in fully developed bones, where labeling of Sema-3A signaling molecules is abundant. Nerve markers PGP9.5 and VIP were also expressed in the same fashion in dd/ff vs WT, only in the perichondrium at E14, and in all the bone tissue at E18. Expression patterns of those molecules were very similar to what we have previously described in rat (Gomez et al., 2005), although they seemed to be set at earlier developmental stages in mice. While confirming in another species that the Sema-3A signaling network is well positioned to regulate bone development and innervation in mice, our data do not show any influence of mechanical unloading on the development of bone innervation during fetal life at these stages of development, at least in terms of general nerve fiber density and distribution. However, an effect restricted to a specific subpopulation of nerve fibers would be too discrete to be detected with the general nerve markers used in our study.

In summary, although we document an altered shape and increased cellular activity of long bones and a hypomineralization of the skeleton, we have not found any evidence for gross anatomical defects of bone development in dd/ff mice, and specifically no alteration nor delay in endochondral ossification and bone innervation. Some of the effects observed have been well characterized as consequences of bone unloading. Others, for instance morphological features of dd/ff mice, may reflect regulatory effects specific to bone development in

hypokinetic conditions which remain to be confirmed by more detailed studies. The lack of curvature and the uniform diameter of the humerus in dd/ff mice suggest that much of the basic shape of a bone element that was thought to be determined by genetic influences is influenced, *in utero,* by mechanical strain. The effect of movement and the bone strain induced by muscle activity appears to be to shape the metaphysis to make broader joint surfaces and to induce curvature which has benefits on predictability of failure (Bertram & Biewener, 1988).

Aknowledgements

The authors thank INSERM Unit 403, specifically Dr Philippe Clézardin for the use of histology material and Brigitte Burt-Pichat for technical advice. L.M. and L.V. are funded by the « Institut National de la Santé et de la Recherche Médicale » (INSERM), Paris, France. C.G. was funded by a postgraduate fellowship from the Rhône-Alpes Region, France.

Figure Legends

Figure 1: Skeletal architecture at E18 of dd/ff and WT mice. A: Images of pups after removal of the skin over the thorax. In dd/ff fetuses, the gaunt outline of the limb is striking because of the absence of the bulk of the leg musculature, and the characteristic appearance of the lung lobes is visible because of the absence of ribs; bar = 2mm. B: Whole mount preparation of forelimbs for skeletal morphometry; bar = 1mm. C: μCT 3D reconstruction of the skeletal architecture of wild type (WT) and mutant (dd/ff) mice.

Figure 2: Structural analysis of dd/ff and WT mouse femurs at E18. A: μCT 3D reconstruction and 2D longitudinal and transversal imaging (medial section) of mineralized femur shaft. B: Measurement of width (2D) and cortical thickness (3D) of femur shafts; *: $p \leq 0.05$ vs WT, Mann-Whitney U test. See Material and Methods for details.

Figure 3: Development and cellular dynamics of the appendicular skeleton of dd/ff and WT mice at E18. A and B: Von-Kossa staining of digits in longitudinal section; arrows: hypertrophic chondrocytes in the second phalanx; arrowhead: incipient mineralization. C and D: Goldner's trichrome of hindlimb femurs; stars: skeletal muscle location. E and F: Histoenzymology of TRACP in non counterstained sections of hindlimb tibia (T) and fibula (F). Dashed lines delimit the growth plates; double arrows locate the cortical envelopes; arrowheads: TRACP positive osteoclasts. All bars = 50μm. G: Quantification of osteoclasts on longitudinal sections of tibias and fibulas. **: $p<0.01$ vs WT, ANOVA2 with Bonferroni post-test. See Material and Methods for details.

Figure 4: Nerve marker expression during endochondral ossification of dd/ff and WT limb bones. A: dd/ff, E14, PGP 9.5 expression in the perichondrium, dotted line circle: nerve fibers. B: WT, E14 VIP expression in the perichondrium. C: WT, E18, PGP 9.5 expression in the periosteum and the metaphysis, D: dd/ff, E18, PGP 9.5 expression in the diaphysis. E: WT, E18, negative control (rabbit serum). F: WT, E18, VIP expression in the metaphysis. G: WT, E18, VIP expression in the diaphysis. Arrows: blood vessels, arrowheads: osteoblasts, C: Cartilage, P: Periosteum, PC: Perichondrium, PO: Periosteal osteoblasts. All bars = 20μm.

Figure 5: Expression of Semaphorin-3A signaling molecules during endochondral ossification of dd/ff and WT limb bones. A: dd/ff, E14, Sema-3A expression in the forearm, RC: resting chondrocytes, HC: hypertrophic chondrocytes. B: dd/ff, E18, Sema-3A expression in the metaphysis. C: WT, E18, Sema-3A expression in the diaphysis. D: WT, E18, NP-1, metaphysis. E: dd/ff, E18, NP-1, diaphysis. F: WT, E18, Plx-A1, diaphysis. G: dd/ff, E18, Plx-A1, metaphysis. H: WT, E18, Plx-A2, diaphysis. I: dd/ff, E18, Plx-A2, metaphysis. J: WT, E18, Plx-A3, diaphysis. K: dd/ff, E18, Plx-A3, diaphysis. L: WT, E18, negative control (goat serum). Arrows: blood vessels, Arrowheads: nerve fibers, C: cartilage, P: periosteum, short arrows: osteoblasts. Bar = 50μm in A, 20μm in all others.

Table 1: Differences in forelimb bone dimensions of WT and dd/ffmice at E18. Values (in mm) are mean±SEM of 6 fetuses.

Dimension	WT	dd/ff	p[1]
Humerus length[2]	2.95 ± 0.13	2.9 ± 0.11	NS
Humerus diameter[3]	0.43 ± 0.025	0.48 ± 0.02	<0.05
Humeral diameter inc. DT[4]	0.65 ± 0.03	0.5 ± 0.02	<0.01
Humeral head	0.7 ± 0.02	0.5 ± 0.02	<0.01
Humeral condyles	0.7 ± 0.03	0.46 ± 0.02	<0.01
Ulna total length	3.4 ± 0.14	3.0 ± 0.1	<0.05
Ulna shaft length	3.1 ± 0.12	2.9 ± 0.2	NS
Ulna diameter	0.29 ± 0.01	0.3 ± 0.01	NS
Radius length	2.4 ± 0.1	2.3 ± 0.12	NS
Radius diameter	0.27 ± 0.01	0.28 ± 0.01	NS
Height T8	0.4 ± 0.02	0.36 ± 0.25	NS
Deltoid tuberosity size	0.32 ± 0.01	0.04 ± 0.002	<0.01
Olecranon length	0.3 ± 0.02	0.1 ± 0.01	<0.05

[1]: Mann-Whitney U test. [2]: Bone lengths are from one articular surface to the other except in the ulna where the length is from the olecranon to the distal articular surface. [3]: Humerus diameter was taken below the position of the deltoid tuberosity; radius and ulna diameters were taken at midshaft. [4]: DT: deltoid tuberosity, T8: eighth thoracic vertebra, NS: non significant.

Table 2: Linear attenuation coefficients of whole femur and cortical area in WT and dd/ff mice at E18. Values are Mean+SEM of 5 WT and 4 dd/ff fetuses.

Region of interest:	WT	dd/ff	p[1]
Whole Femur	1.92 ± 0.012	1.86 ± 0.012	<0.05
Bone collar	2.13 ± 0.009	2.05 ± 0.027	<0.05
p	<0.01	<0.05	

[1]: Mann-Whitney U test.

Bibliography

Basso N, Bellows CG, Heersche JN (2005) Effect of simulated weightlessness on osteoprogenitor cell number and proliferation in young and adult rats. *Bone* **36,** 173-183.

Bertram JE, Biewener AA (1988) Bone curvature: sacrificing strength for load predictability? *J Theor Biol* **131,** 75-92.

Biewener AA, Bertram JE (1994) Structural response of growing bone to exercise and disuse. *J Appl Physiol* **76,** 946-955.

Bjurholm A, Kreicbergs A, Brodin E, Schultzberg M (1988) Substance P- and CGRP-immunoreactive nerves in bone. *Peptides* **9,** 165-171.

Bliziotes M, Gunness M, Eshleman A, Wiren K (2002) The role of dopamine and serotonin in regulating bone mass and strength: studies on dopamine and serotonin transporter null mice. *J Musculoskelet Neuronal Interact* **2,** 291-295.

Chen H, Blackburn WR, Wertelecki W (1995) Fetal akinesia and multiple perinatal fractures. *Am J Med Genet* **55,** 472-477.

Chenu C (2004) Role of innervation in the control of bone remodeling. *J Musculoskelet Neuronal Interact* **4,** 132-134.

Cherruau M, Facchinetti P, Baroukh B, Saffar JL (1999) Chemical sympathectomy impairs bone resorption in rats: a role for the sympathetic system on bone metabolism. *Bone* **25,** 545-551.

Ducy P, Amling M, Takeda S, et al. (2000) Leptin inhibits bone formation through a hypothalamic relay: a central control of bone mass. *Cell* **100,** 197-207.

Edoff K, Hellman J, Persliden J, Hildebrand C (1997) The developmental skeletal growth in the rat foot is reduced after denervation. *Anat Embryol (Berl)* **195,** 531-538.

Elefteriou F, Karsenty G (2004) [Bone mass regulation by leptin: a hypothalamic control of bone formation]. *Pathol Biol (Paris)* **52,** 148-153.

Gomez C, Burt-Pichat B, Mallein-Gerin F, et al. (2005) Expression of Semaphorin-3A and its receptors in endochondral ossification: potential role in skeletal development and innervation. *Dev Dyn* **234,** 393-403.

Grano M, Mori G, Minielli V, et al. (2002) Rat hindlimb unloading by tail suspension reduces osteoblast differentiation, induces IL-6 secretion, and increases bone resorption in ex vivo cultures. *Calcif Tissue Int* **70,** 176-185.

Gronblad M, Liesi P, Korkala O, Karaharju E, Polak J (1984) Innervation of human bone periosteum by peptidergic nerves. *Anat Rec* **209,** 297-299.

Hohmann EL, Elde RP, Rysavy JA, Einzig S, Gebhard RL (1986) Innervation of periosteum and bone by sympathetic vasoactive intestinal peptide-containing nerve fibers. *Science* **232,** 868-871.

Hosseini A, Hogg DA (1991) The effects of paralysis on skeletal development in the chick embryo. I. General effects. *J Anat* **177,** 159-168.

Janckila AJ, Li CY, Lam KW, Yam LT (1978) The cytochemistry of tartrate-resistant acid phosphatase. Technical considerations. *Am J Clin Pathol* **70,** 45-55.

Kaul A, Koster M, Neuhaus H, Braun T (2000) Myf-5 revisited: loss of early myotome formation does not lead to a rib phenotype in homozygous Myf-5 mutant mice. *Cell* **102,** 17-19.

Kawashima K, Yamaguchi A, Shinki T, et al. (1995) Microgravity generated by space flight has little effect on the growth and development of chick embryonic bone. *Biol Sci Space* **9,** 82-94.

Kondo H, Nifuji A, Takeda S, et al. (2005) Unloading induces osteoblastic cell suppression and osteoclastic cell activation to lead to bone loss via sympathetic nervous system. *J Biol Chem* **280,** 30192-30200.

Lanyon LE (1980) The influence of function on the development of bone curvature. An experimental study in the rat. *J Zool Lond* **192,** 457-466.

Levasseur R, Sabatier J, Potrel-Burgot C, et al. (2003) Sympathetic nervous system as transmitter of mechanical loading in bone. *Joint Bone Spine* **70,** 515-519.

McKee MD, Nanci A, Landis WJ, et al. (1991) Effects of fixation and demineralization on the retention of bone phosphoprotein and other matrix components as evaluated by biochemical analyses and quantitative immunocytochemistry. *J Bone Miner Res* **6,** 937-945.

Mosley JR, March BM, Lynch J, Lanyon LE (1997) Strain magnitude related changes in whole bone architecture in growing rats. *Bone* **20,** 191-198.

O'Shea PJ, Harvey CB, Suzuki H, et al. (2003) A thyrotoxic skeletal phenotype of advanced bone formation in mice with resistance to thyroid hormone. *Mol Endocrinol* **17,** 1410-1424.

Palacios J, Rodriguez JI, Ruiz A, et al. (1992) Long bone development in extrinsic fetal akinesia: an experimental study in rat fetuses subjected to oligohydramnios. *Teratology* **46,** 79-84.

Pitsillides AA (2006) Early effects of embryonic movement: 'a shot out of the dark'. *J Anat* **208,** 417-431.

Rodriguez JI, Garcia-Alix A, Palacios J, Paniagua R (1988) Changes in the long bones due to fetal immobility caused by neuromuscular disease. A radiographic and histological study. *J Bone Joint Surg Am* **70,** 1052-1060.

Rot-Nikcevic I, Reddy T, Downing KJ, et al. (2006) Myf5-/- :MyoD-/- amyogenic fetuses reveal the importance of early contraction and static loading by striated muscle in mouse skeletogenesis. *Dev Genes Evol* **216,** 1-9.

Rudnicki MA, Schnegelsberg PN, Stead RH, et al. (1993) MyoD or Myf-5 is required for the formation of skeletal muscle. *Cell* **75,** 1351-1359.

Sandhu HS, Herskovits MS, Singh IJ (1987) Effect of surgical sympathectomy on bone remodeling at rat incisor and molar root sockets. *Anat Rec* **219,** 32-38.

Schneider D, Hofmann MT, Peterson JA (2002) Diagnosis and treatment of Paget's disease of bone. *Am Fam Physician* **65,** 2069-2072.

Serre CM, Farlay D, Delmas PD, Chenu C (1999) Evidence for a dense and intimate innervation of the bone tissue, including glutamate-containing fibers. *Bone* **25,** 623-629.

Sisask G, Bjurholm A, Ahmed M, Kreicbergs A (1995) Ontogeny of sensory nerves in the developing skeleton. *Anat Rec* **243,** 234-240.

Sisask G, Bjurholm A, Ahmed M, Kreicbergs A (1996) The development of autonomic innervation in bone and joints of the rat. *J Auton Nerv Syst* **59,** 27-33.

Spencer GJ, Hitchcock IS, Genever PG (2004) Emerging neuroskeletal signalling pathways: a review. *FEBS Lett* **559,** 6-12.

Takeda S, Karsenty G (2001) Central control of bone formation. *J Bone Miner Metab* **19,** 195-198.

Thompson DD, Rodan GA (1988) Indomethacin inhibition of tenotomy-induced bone resorption in rats. *J Bone Miner Res* **3,** 409-414.

Uhthoff HK, Jaworski ZF (1978) Bone loss in response to long-term immobilisation. *J Bone Joint Surg Br* **60-B,** 420-429.

Vico L, Collet P, Guignandon A, et al. (2000) Effects of long-term microgravity exposure on cancellous and cortical weight-bearing bones of cosmonauts. *Lancet* **355,** 1607-1611.

Wada S, Kojo T, Wang YH, et al. (2001) Effect of loading on the development of nerve fibers around oral implants in the dog mandible. *Clin Oral Implants Res* **12,** 219-224.

Walker LM, Preston MR, Magnay JL, Thomas PB, El Haj AJ (2001) Nicotinic regulation of c-fos and osteopontin expression in human-derived osteoblast-like cells and human trabecular bone organ culture. *Bone* **28,** 603-608.

Weinreb M, Rodan GA, Thompson DD (1989) Osteopenia in the immobilized rat hind limb is associated with increased bone resorption and decreased bone formation. *Bone* **10,** 187-194.

Whedon GD (1984) Disuse osteoporosis: physiological aspects. *Calcif Tissue Int* **36 Suppl 1,** S146-150.

Wolff J (1892) *The law of bone remodeling,* Verlag Hirschwald, Berlin.

Wronski TJ, Morey ER (1982) Skeletal abnormalities in rats induced by simulated weightlessness. *Metab Bone Dis Relat Res* **4,** 69-75.

Yonezu H, Takata S, Shibata A (2004) Effects of unilateral sciatic neurectomy on growing rat femur as assessed by peripheral quantitative computed tomography, Fourier transform infrared spectroscopy and bending test. *J Med Invest* **51,** 96-102.

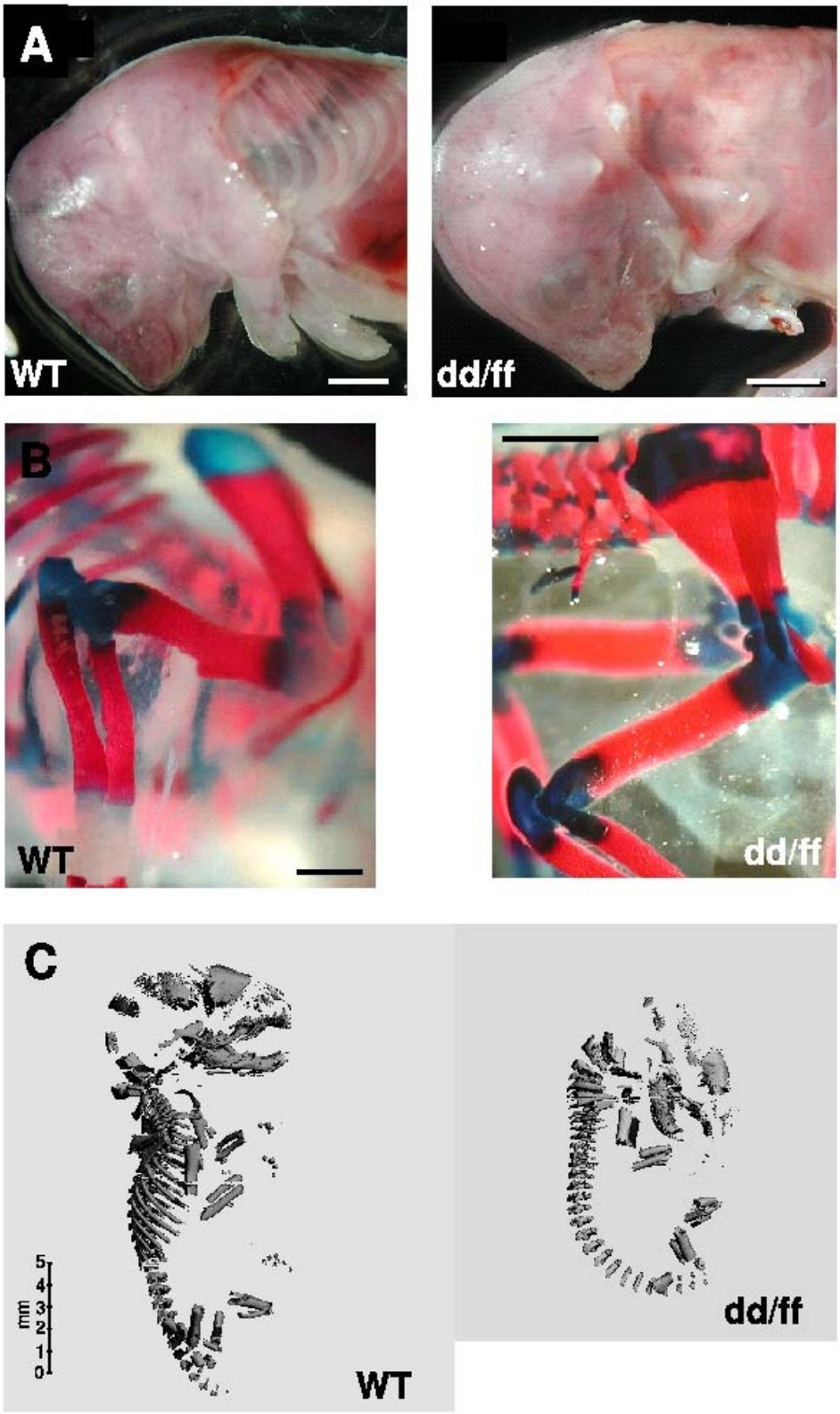

Gomez et al., Fig. 1

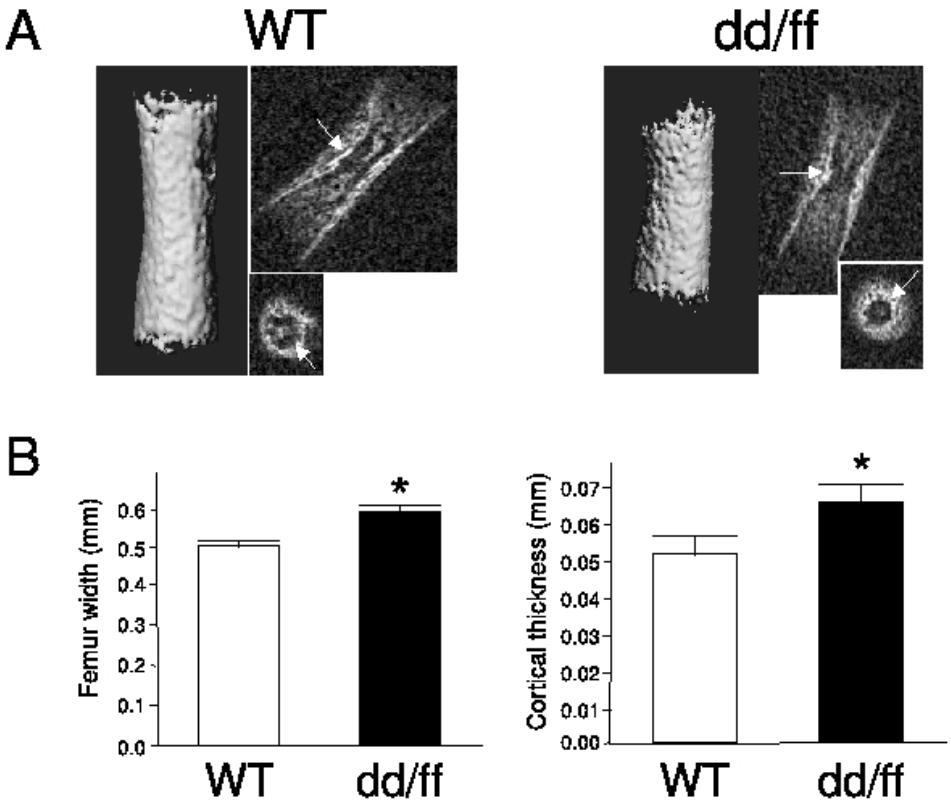

Gomez et al., Fig. 2

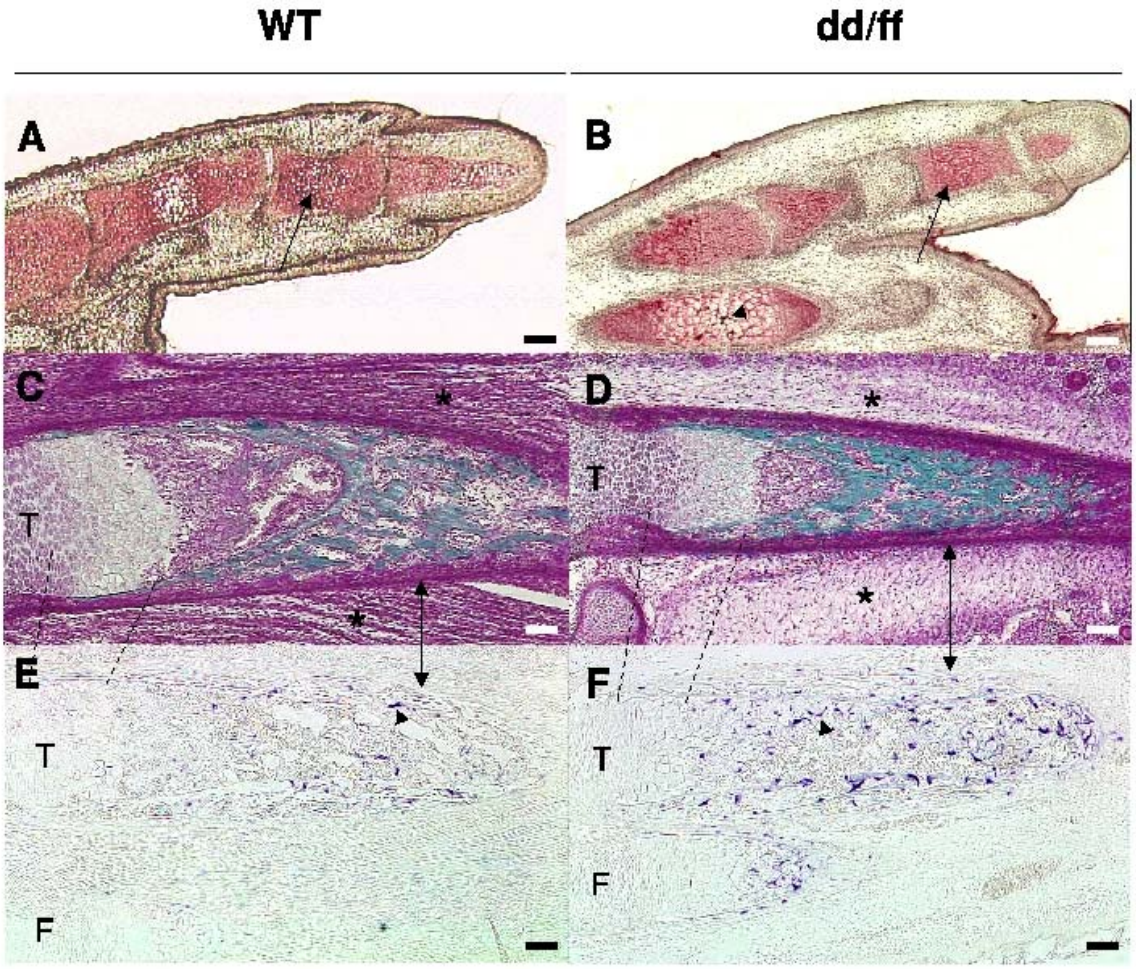

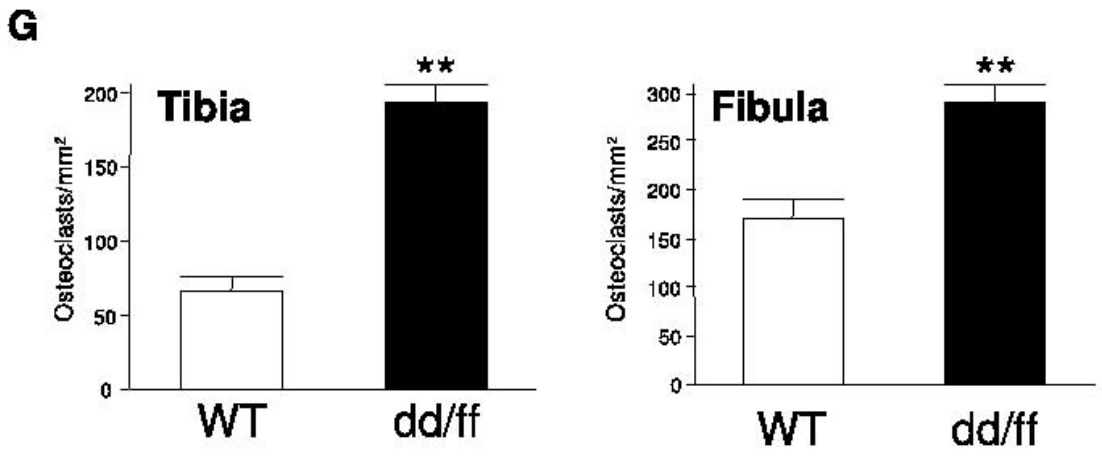

Gomez et al., Fig. 3

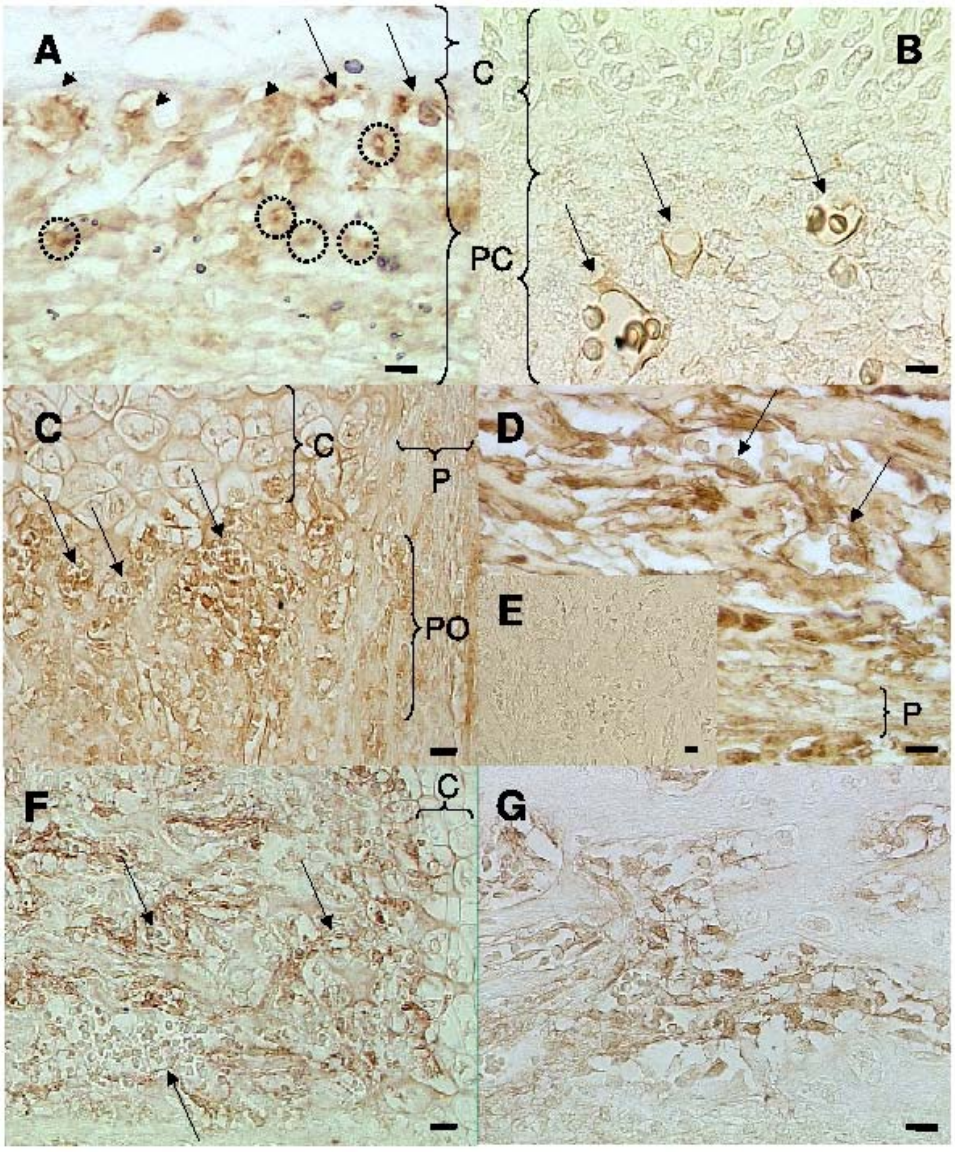

Gomez et al., Fig. 4

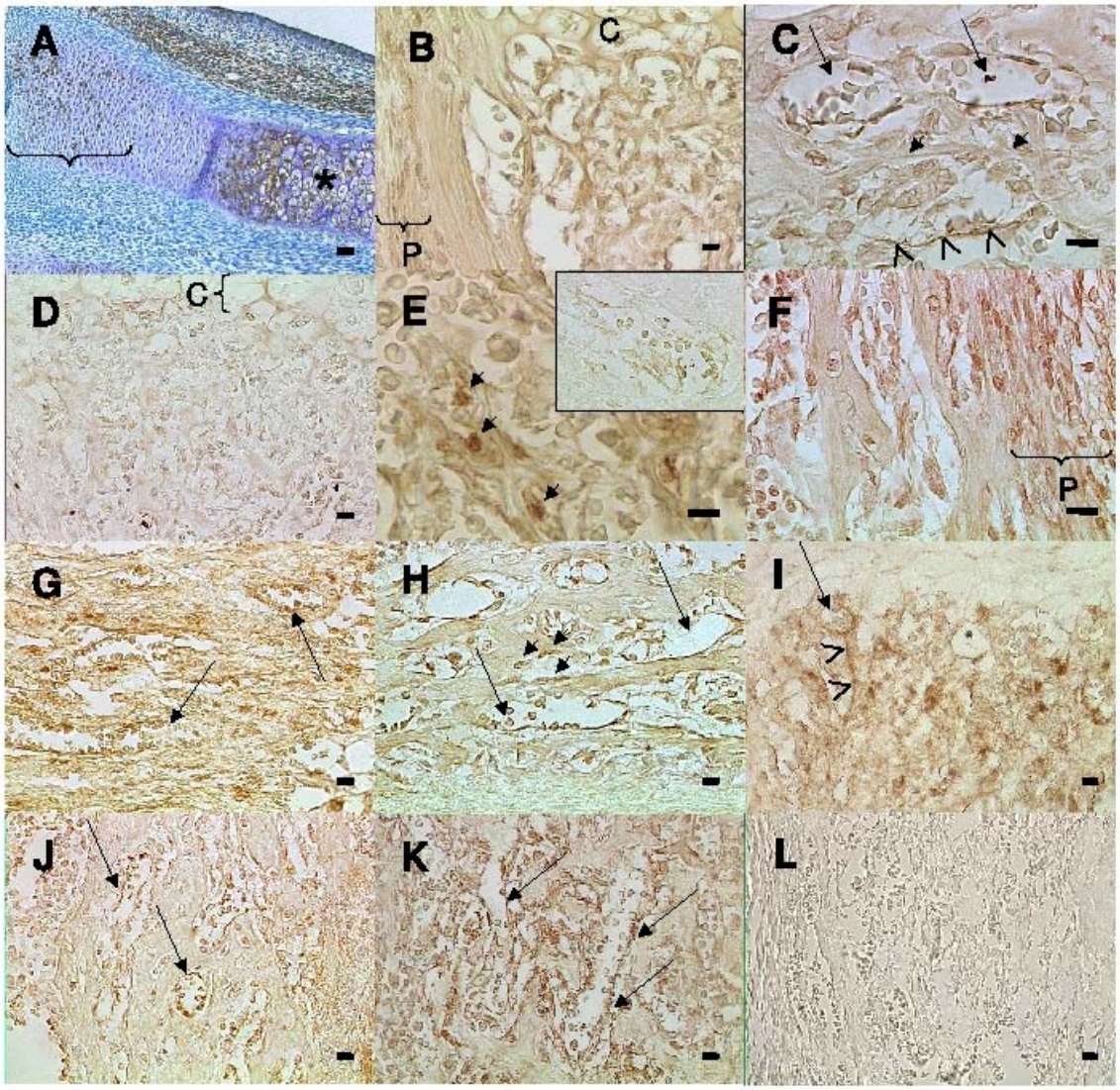

Gomez et al., Fig. 5